

On the use of lithogenic tracer measurements in aerosols to constrain dust deposition fluxes to the ocean southeast of Australia.

Claudia Hird^{a*}, Morgane M.G. Perron^{ab*}, Thomas M. Holmes^{cd}, Scott Meyerink^e, Christopher Nielsen^a, Ashley T. Townsend^d, Patrice de Caritat^e, Michal Strzelec^a, Andrew R. Bowie^{ac}

^a Institute for Marine and Antarctic Studies (IMAS), University of Tasmania, Battery Point, Tasmania, Australia.

^b Université de Brest - UMR 6539 CNRS/UBO/IRD/Ifremer, Laboratoire des sciences de l'environnement marin (LEMAR) - Institut Universitaire Européen de la Mer - Rue Dumont D'Urville, 29280 Plouzané, France

^c Australian Antarctic Program Partnership (AAPP), University of Tasmania, Battery Point, Tasmania, Australia.

^d Central Science Laboratory, University of Tasmania, Hobart, Tasmania, Australia

^e John de Laeter Centre, Curtin University, Bentley WA 6845, Australia

* These authors contributed equally to this work.

Correspondence to: Morgane M.G. Perron, morgane.perron@univ-brest.fr

Abstract

1 Australia contributes a significant amount of dust-borne nutrients (including iron) to the Southern
2 Ocean, which can stimulate marine primary productivity. A quantitative assessment of the
3 variability of dust fluxes from Australia to the surrounding ocean is therefore important for
4 investigating the impact of atmospheric deposition on the Southern Ocean's carbon cycle. In this
5 study, lithogenic trace metals (aluminium, iron, thorium and titanium) contained in aerosols
6 collected between 2016 and 2021 from kunanyi/Mount Wellington in lutruwita/Tasmania
7 (Australia) were used to estimate dust deposition fluxes. Lithogenic fluxes were calculated using
8 each tracer individually, as well as an average using all four tracers. This latter approach enabled
9 an assessment of the uncertainty associated with flux calculations using only individual tracers.
10 Elemental ratios confirmed the lithogenic nature of each tracer in aerosols when compared with
11 both Australian soil samples and the average Earth's upper continental crust. [Lithogenic flux](#)
12 [estimates showed annual dust deposition maxima during the austral summer, following the](#)
13 [Australian dust storm season, and annual minimum deposition flux over winter. The data provided](#)

14 [here will help to constrain model estimates of southern hemisphere atmospheric deposition fluxes](#)
15 [and their subsequent impact on global ocean biogeochemical cycles.](#)

16 ▾

17 **Environmental significance / Plain language summary**

18 Dust deposition flux was investigated in lutruwita/Tasmania, Australia, between 2016 and 2021.
19 Results show that the use of direct measurement of aluminium, iron, thorium and titanium in
20 aerosols to estimate average dust deposition fluxes limits biases associated with using single
21 elements. Observations of dust deposition fluxes in the Southern Hemisphere are critical to
22 validate model outputs and better understand the seasonal and interannual impacts of dust
23 deposition on biogeochemical cycles.

24 **1. Introduction**

25 Lithogenic mineral particles such as iron oxyhydroxides, kaolinite, illite and smectite are
26 commonly entrained into the atmosphere (Cudahy et al., 2016) following the erosion of the Earth's
27 Upper Continental Crust (UCC) (Crawford et al., 2021). Such dust particles are the primary source
28 of trace metals including aluminium (Al), iron (Fe), thorium (Th) and titanium (Ti) to the
29 atmosphere, which can therefore be used as tracers of aeolian lithogenic inputs to the ocean (Baker
30 et al., 2020). Dust carries important nutrients, including Fe, to marine ecosystems, feeding primary
31 producers (Mackie et al., 2008). Due to the current lack of field observations on the concentrations
32 of aeolian trace metals and their corresponding dust deposition fluxes, large uncertainties remain
33 regarding how and to what extent dust supply fertilises key oceanic regions such as the Southern
34 Ocean with vital nutrients. This leads to a poor understanding of the impact of dust deposition on
35 the biological carbon pump.

36
37 The amount of dust entrained into the atmosphere depends on soil surface roughness, vegetation
38 and coverage, on particle size, composition, and moisture content, and on local conditions such as
39 wind speed and rainfall, which change both regionally and seasonally (Mahowald et al., 2009). Air
40 masses can carry dust over thousands of kilometres before particles return to land or fall onto the
41 surface ocean (Mackie et al., 2008). Atmospheric deposition of dust to the open ocean has been
42 demonstrated to act as a key supplier of vital macro- and micro-nutrients (such as Fe) to the marine
43 ecosystem (Mackie et al., 2008; Weis et al., 2024). For example, during the austral summer 2019-

a supprimé: Determined lithogenic flux estimates were consistent with a regular dust deposition peak during the austral summer, in line with the dust storm season in the southeast of Australia, and a low atmospheric deposition in winter. ocean This study provides an insight into the seasonal and interannual variability of dust deposition fluxes from the southeast of Australia based on aerosol sample measurements. This information will enhance our understanding of nutrient-bearing dust deposition to the Australian sector of the Southern Ocean and may prove useful in refining modelling estimates of southern hemisphere atmospheric deposition fluxes and their subsequent impact on global biogeochemical cycles.⁴

57 2020, nutrient supply from large dust-containing bushfire emissions (Perron et al., 2022; Hamilton
58 et al., 2022) was identified as the main trigger of a large and long-lasting phytoplankton bloom in
59 the South Pacific Ocean (Weis et al., 2022).

60

61 Field and modelling approaches to estimating dust deposition both offer various benefits and
62 drawbacks. Field observations at sea are influenced by local environmental conditions (i.e.,
63 weather, surface ocean properties) and are not representative of the large scale or long-term
64 atmospheric deposition trends (Anderson et al., 2016). Time-series stations on land can overcome
65 the issue of temporal coverage but may not be representative of atmospheric loading and
66 deposition over remote oceanic regions. To date, global models are not capable of reproducing
67 atmospheric concentrations of trace metals transported in dust to remote areas and cannot
68 accurately quantify particle settling rates (Anderson et al., 2016). Considering the Southern
69 Hemisphere, model estimates tend to overestimate total dust emission at the source and
70 underestimate soluble trace element deposition fluxes over the ocean (Anderson et al., 2016; Ito et
71 al., 2020). To reduce uncertainty in dust deposition fluxes to the open ocean it is essential to
72 validate model fluxes using field-based observations. Long-term atmospheric observatories,
73 particularly near the coasts, are attracting increasing interest from the scientific community as a
74 platform to better understand seasonal to interannual patterns of deposition events in addition to
75 shipboard observations and satellite estimates (Perron et al., 2022; De Deckker, 2019).

76

77 In Australia, the large spatial heterogeneity of soil types and the highly episodic nature of weather
78 events such as droughts, bushfires and dust storms make it particularly difficult to model dust
79 deposition fluxes (Mackie et al., 2008), [though modern dust emissions from South Australia have](#)
80 [been observed as far as the snow sheet of inner Antarctica \(Vecchio et al., 2024\).](#) A main source
81 of trace metals to the Australian sector of the Southern Ocean is dust carried from kati thanda/Lake
82 Eyre and dhungala-barka/Murray-Darling geological basins (De Deckker, 2019). The typical dust
83 storm season in Australia spans from September to November (austral spring), with the most
84 extreme storms occurring in September (O’Loingsigh et al., 2017). The dust season can extend
85 through the austral summer due to bushfires (and postfire unvegetated ground) across southern
86 Australia (Hamilton et al., 2022). In a study conducted by Perron et al. (2022), atmospheric
87 concentrations of mineral dust and associated lithogenic tracers (Al, Fe and Ti) were reported to

a supprimé: though. mhave been the snow sheet of

89 be 2.5-fold higher, on average, during fire events compared to days not impacted by bushfires in
90 lutruwita/Tasmania, Australia.

91

92 Dust deposition fluxes reported by different models range over an order of magnitude (from 0.55
93 to 5.48 mg m⁻² d⁻¹) over the Southern Ocean region southeast of Australia (Mahowald et al., 2006;
94 Weis et al., 2024). Different methods have also been used to estimate dust deposition fluxes from
95 field samples. While broadly used in air pollution studies (Bindu et al., 2016), total aerosol loading
96 measurements based on gravimetry does not enable the discrimination of atmospheric sources
97 (e.g., dust vs anthropogenic). In addition, such a method is not compatible with atmospheric trace
98 metal studies, where strict protocol requires minimal filter handling to prevent contamination, from
99 the analysis of a single tracer element, for example Al or Th, in aerosol samples and in seawater
100 (Anderson et al., 2016). However, single element dust flux estimates are subject to anomalous data
101 stemming from contamination, deviation from the mean UCC, or preferential mineralization
102 following a particular laboratory protocol. Recently, the analysis of four lithogenic tracers
103 (namely, Al, Fe, Th, and Ti) in marine sinking particles collected at the Southern Ocean Time-
104 Series (SOTS) mooring station (140°E, 47°S) were used to calculate an average ‘multi-tracer’
105 estimate of dust deposition fluxes to surface waters of the subantarctic ocean south of Australia
106 (Traill et al., 2022). The latter field-based flux estimates showed good agreement with remotely
107 sensed proxies of dust transport and modelled deposition estimates. Elemental ratio analysis in the
108 same sediment trap samples suggested that lithogenic material from southeastern Australia was
109 the most likely source of Al, Fe, Th and Ti to this area of the Southern Ocean (Traill et al., 2022).

110

111 In this study, the analysis of the same four lithogenic tracers (Al, Fe, Th, and Ti) was performed
112 in aerosol samples collected at the kunanyi/Mount Wellington time-series sampling station in
113 southern lutruwita/Tasmania (Australia). Dust deposition fluxes were estimated from both
114 individual tracer concentrations and using the multi-tracer approach used by Traill et al. (2022).
115 Here we report a 5-year (2016-2021) time-series of dust deposition flux estimates downwind of
116 the south-eastern Australian dust path, at one of the gateway to the Southern Ocean. The suitability
117 of the four metals as lithogenic tracers was also verified by comparing elemental ratios (relative to
118 Al) in the aerosol samples to the average topsoil composition in Australia (this study) and to the
119 averaged UCC composition (McLennan et al., 2001).

a **supprimé**: Different methods have been used to estimate dust deposition fluxes

122

123 2. Material and methods

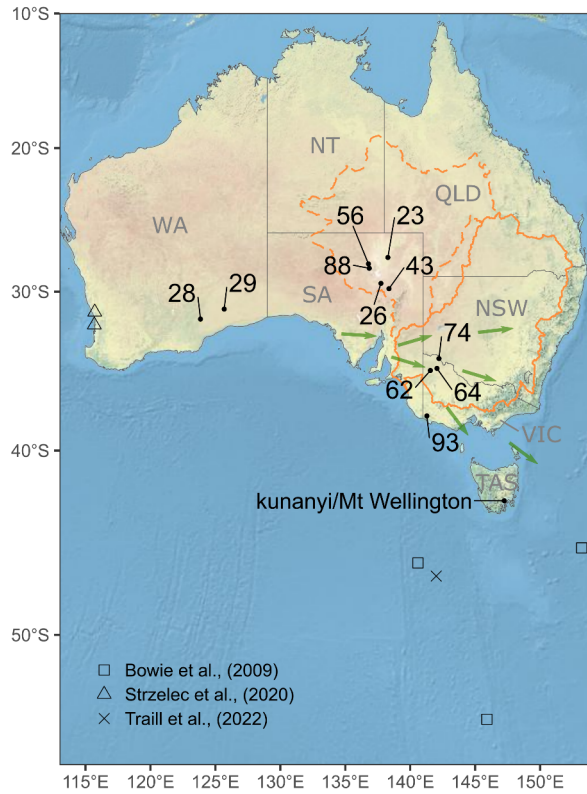
124 2.1 Aerosol collection and study site

125 kunanyi/Mount Wellington overlooks Hobart, the capital city of the Australian island state of
126 lutruwita/Tasmania. The mountain is in a strategic position for sampling one of the three major
127 atmospheric pathways in Australia (Baddock et al. 2015; Bowler 1976), where air-masses from
128 mainland Australia are transported south-eastwards over lutruwita/Tasmania (and our sampling
129 site, Figure 1) before reaching the Southern Ocean. This study uses aerosol filters collected on a
130 HiVOL 3000 air particulate sampler (Ecotech, Acoem, Melbourne, Australia) positioned at 1,271
131 m above sea level, on the summit of kunanyi/Mount Wellington. Filter samples have been
132 collected for Total Suspended Particulates (TSP) since September 2016, with each sample
133 representing a period ranging from a few days to 2 weeks, depending on weather conditions and
134 specific weather events, and allowing for sampler servicing and calibration. [Samples suspected for
135 contamination or that were significantly wet at the time of recovery were discarded and sampling
136 was suspended in the winter time of 2017, 2018 and 2019 for operational reasons. As a result, 125
137 aerosol samples were selected from the kunanyi/Mount Wellington atmospheric time-series
138 collection for this study \(November 2016 - February 2022\). The origin and concentration of aerosol
139 Fe in 80 samples from this dataset was previously reported in Perron et al. \(2022\), however the](#)

a mis en forme : Anglais (AUS)

140 present study differs in using total concentrations of Fe, Al, Th and Ti to calculate atmospheric
 141 (dust) deposition fluxes and the associated seasonal and interannual trends at the sampling station.
 142

a supprimé: for operational reasons For this study, 125 aerosol samples were selected from the kunanyi/Mount Wellington atmospheric particle time-series collection (November 2016 - February 2022). The origin and concentration of aerosol Fe in 80 samples from this dataset was previously reported in Perron et al. (2022), however the present study differs in using total concentrations of Fe, Al, Th and Ti to calculate atmospheric (dust) deposition fluxes and the associated seasonal and interannual trends at the sampling station.



143
 144 **Figure 1.** Location of the aerosol sampling station at kunanyi/Mount Wellington in Tasmania (TAS). Black
 145 dots display the locations of selected NGSAs soil samples in the Australian states of Western Australia
 146 (WA), South Australia (SA) and Victoria (VIC) with identification numbers annotated (see Table S2).
 147 Prevailing dust pathways of southeast Australia are displayed as green arrows adapted from Sprigg (1982)
 148 and Mackie et al. (2008). The kati thanda/Lake Eyre (dashed line) and dhungala-barka/Murray-Darling
 149 (solid line) geological basins are delineated in orange. Location of previous field studies that estimated dust
 150 deposition fluxes are also indicated.

151
 152 2.2 Aerosol leaching protocol
 153 Laboratory work for aerosol and soil sample processing (sections 2.2 and 2.3) followed
 154 GEOTRACES recommended procedures for ultra-trace sampling and analysis (Cutter et al., 2017).

165 All reagents were ultra-high purity (UHP) and either purchased (Baseline, SeaStar Chemicals) or
166 distilled in-house using instrument quality reagents (IQ grade, SeaStar Chemicals). Whatman W41
167 (203mm x 254mm paper sheets, Sigma-Aldrich) filters were acid washed in a series of 24h
168 hydrochloric acid (0.5 M HCl) baths and rinsed with UHP water to leach any impurities and reduce
169 the impact of the cellulose filter on the analysis of trace elements in aerosols (Perron et al., 2020a).
170 Perron et al. (2020a) suggested a 3-step leaching method to define trace metal concentrations and
171 solubility in aerosols taken from land-based stations in Australia (Strzelec et al., 2020a, 2020b)
172 and on research vessels operating around Australia and in the Southern Ocean (Perron et al., 2020b,
173 2021). Although samples were collected and analysed in batch over several years, the collection
174 and analysis of each batch of samples follow the same protocol and the resulting data was quality-
175 controlled against blanks, replicate analysis and Certified Reference Materials (Table S1).

176
177 One sub-sample of 47mm diameter was cut off each aerosol filter sheet collected at our sampling
178 station using a sharp titanium punch cutter (Perron et al., 2020). Sub-samples were successively
179 leached using UHP water (Milli-Q®, 18.2 MΩ) and 1.1 M ammonium acetate (10 mL, pH 4.7).
180 The remaining filter residue was then digested using a mixture of concentrated nitric acid (HNO₃,
181 1 mL) and concentrated hydrofluoric acid (HF, 0.25 mL) at 120°C for 12 hours (Perron et al.,
182 2020a). The sum of all three steps in the protocol provided the total concentration data for each
183 lithogenic tracer in aerosols which is used in this study (Perron et al., 2020a). Satisfactory
184 recoveries (>90%) were obtained for Al, Fe and Ti when applying the total metal digestion step of
185 the protocol to two reference materials, the Arizona Test Dust (ATD) (Morton et al., 2013) and
186 the GeoPT13 certified Koeln loess (International Association of Geoanalysts) (Potts et al., 2003)
187 (supplementary Table S1). A smaller recovery of 87% (using only certified reference material)
188 obtained for Th highlights the unique extraction and stability chemistry of the metal which our
189 protocol is not optimised for. Thorium concentrations are therefore likely to be slightly
190 underestimated in this study as discussed in section 3. Only total metal concentrations are
191 discussed in the present study.

192 193 2.3 Atmospheric deposition flux estimates

194 The total concentration of each lithogenic tracer in our samples was used to calculate single tracer-
195 dust deposition flux estimates. Additional measurements on the collected aerosols (e.g.: carbon

a supprimé: A

a supprimé: samples were

a supprimé: 7%

a supprimé: be

200 and major ion analysis) were not available for this study, so intrinsic calculation of the total aerosol
201 mass on each individual aerosol filter using these parameters was not possible.

202 In addition, due to the lack of necessary meteorological data to estimate particle deposition
203 velocities specific to our study site, a single coarse particle deposition velocity of 0.2 cm s^{-1} was
204 applied to trace metal-bearing dust deposition estimates based on the literature in similar study
205 regions (Baker et al., 2017; Perron et al., 2020b; Winton et al., 2015). In this study, “F(X)” denotes
206 the deposition flux estimate for the individual lithogenic tracer “X”. F(X) (in $\text{mg m}^{-2} \text{ d}^{-1}$) was
207 obtained following equation (1):

$$208 \quad F(X) = C_x * V_d \quad (1)$$

209 where X is the lithogenic tracer – Al, Fe, Th or Ti ; C_x is the total metal concentration (ng m^{-3}) in
210 aerosols and V_d is a constant deposition velocity of 1723 m d^{-1} (0.2 cm s^{-1}). It should be mentioned
211 that a factor of 3 uncertainty was previously attributed to the use of a set deposition velocity as it
212 does not account for specific particle size in different aerosol samples or for specific atmospheric
213 conditions such as humidity and wind speed at the collection time (Baker et al., 2016; Winton et
214 al., 2016; Duce et al, 1991).

215
216 Similar to other studies reported in the literature, a single-tracer dust (lithogenic) deposition flux
217 estimate, $F_{\text{Lith}(X)}$, was calculated by dividing F(X) by the average abundance ($[X]_{\text{UCC}}$, wt%) of the
218 element X in the UCC as reported in McLennan (2001); Al = 8.04%, Fe = 3.5%, Th = 1.07×10^{-3}
219 %, Ti = 0.41% following equation (2).

$$220 \quad F_{\text{Lith}(X)} = \frac{F(X) \times 100}{[X]_{\text{UCC}}} \quad (2)$$

221 While $F_{\text{Lith}(X)}$ estimates are solely based on the analysis of a single lithogenic tracer, a multi-tracer
222 dust deposition flux estimate, F_{LithAv} , was obtained by calculating the average of all four $F_{\text{Lith}(X)}$
223 (equation 3, N=4) for each individual aerosol sample.

$$224 \quad F_{\text{LithAv}} = \frac{\sum F_{\text{Lith}(X)}}{N} \quad (3)$$

225 Multi-tracer F_{LithAv} estimates were calculated using both the reported average UCC composition
226 (McLennan, 2001) and Australian soil measurements (see section 2.4 in this study) as references
227 for comparison.

228
229 2.4 Soil sampling and processing

a supprimé: Due to

a supprimé: w

a supprimé: s

a supprimé: ere

a supprimé: then

a supprimé:

a mis en forme : Non Exposant/ Indice

a mis en forme : Non Exposant/ Indice

a mis en forme : Droite

a mis en forme : Couleur de police : Automatique

236 Eleven topsoil (0-10 cm) samples were selected from the National Geochemical Survey of
237 Australia (NGSA) Project: Geochemical Atlas of Australia (Geoscience Australia), a continental-
238 scale geochemical survey covering most of Australia (Caritat and Cooper, 2011; Caritat, 2022).

239 In this study, soil samples originating from the southern part of Western Australia, from South
240 Australia and from Victoria were selected and analysed (Figure 1) as they likely better represent
241 particles entrained through the south-east Australian dust path towards our sampling station and
242 the Southern Ocean (Baddock et al., 2015, Supplementary Figure S1). These sources include the
243 geological basins of kati thanda/Lake Eyre and dhungala-barka/Murray-Darling. It should be
244 mentioned that no sample from New South Wales was used for this study although a large part of
245 the dhungala-barka/Murray-Darling basin is located in this state.

246
247 Ten milligrams of each soil sample was dry sieved through a 63 µm nylon screen to capture the
248 soil fraction fine enough to be entrained into the atmosphere (Strzelec et al., 2020a). The sieved
249 fraction was then processed through the same sequential leaching method described in section 2.2
250 (Perron et al., 2020a). Aerosol and soil leachates were analysed for a suite of elements, including
251 Al, Fe, Th and Ti, by Sector Field Inductively Coupled Plasma Mass Spectrometry (HR-ICP-MS,
252 Thermo Fisher Scientific, Element 2) at the Central Science Laboratory of the University of
253 Tasmania. Increased spectral resolution was employed to resolve major spectral interference
254 overlaps associated with analysis of Al, Fe and Ti. Further details on the ICP-MS analysis
255 procedure are provided in Perron et al. (2020a).

256

257 2.5 Atmospheric source tracking

258 The ratio between the total concentration of each lithogenic tracer of interest, T(X), and the total
259 Al concentration, T(Al), in individual aerosol samples was calculated and compared to the same
260 ratio in the average UCC reported in McLennan (2001) and in the average topsoil from
261 southeastern Australia (Section 2.3). The so-called enrichment factor (EF, equation 3) was used to
262 ascertain the lithogenic origin of Fe, Th and Ti in this study.

263
$$EF = \frac{\frac{T(X)_{aerosol}}{T(Al)_{aerosol}}}{\frac{T(X)_{UCC}}{T(Al)_{UCC}}} \quad (3)$$

264 Using this approach, an EF value below 10 was considered to indicate a prevailing lithogenic
265 source origin for the metal tracers, while an EF exceeding the threshold value of 10 is associated

a supprimé: A 10 mg aliquot of each soil sample was dry sieved...

268 with an enrichment from non-lithogenic atmospheric sources such as anthropogenic combustion
 269 (Shelley et al., 2015; Perron et al., 2022). Reimann and Caritat (2005) warned about the biases
 270 associated with using a low EF threshold to identify anthropogenic sources due to the natural
 271 variability in the Earth's crust composition, fractionation of elements during their emission to –
 272 and transport within – the atmosphere, and biogeochemical processes during and after aeolian
 273 transport. Here, a high EF threshold of 10 is adopted to account for such variability.

274

275 3. Results and discussion

276 3.1 Evaluating the lithogenic origin of the four tracers in aerosols

277 Enrichment Factors (EF) were calculated for Fe, Th and Ti measured in aerosols, and compared to
 278 the Australian soil samples selected from the NGSa (this study) and compared to averaged UCC
 279 composition from McLennan (2001) (Table 1). Calculated EF values were used to discard
 280 significant contributions of non-lithogenic sources to our lithogenic tracers in kunanyi/Mt
 281 Wellington aerosols as indicated by $EF > 10$. [Metal concentrations in individual NGSa soil samples](#)
 282 [analysed in this study are reported in the supplementary Table S2 \(lithogenic tracers\) and in Table](#)
 283 [S3 \(other analysed trace metals not discussed in this study\).](#)

284

Table 1. Comparison of mean Al, Fe, Th and Ti concentrations measured (ppm) in Australian soil samples (n = 11) compared to concentrations reported in the average UCC by McLennan (2001). Enrichment factors (EFs) calculated for Fe, Th and Ti (using Al as a reference) in aerosols collected at kunanyi/Mount Wellington (n = 125) are also displayed using both crustal references

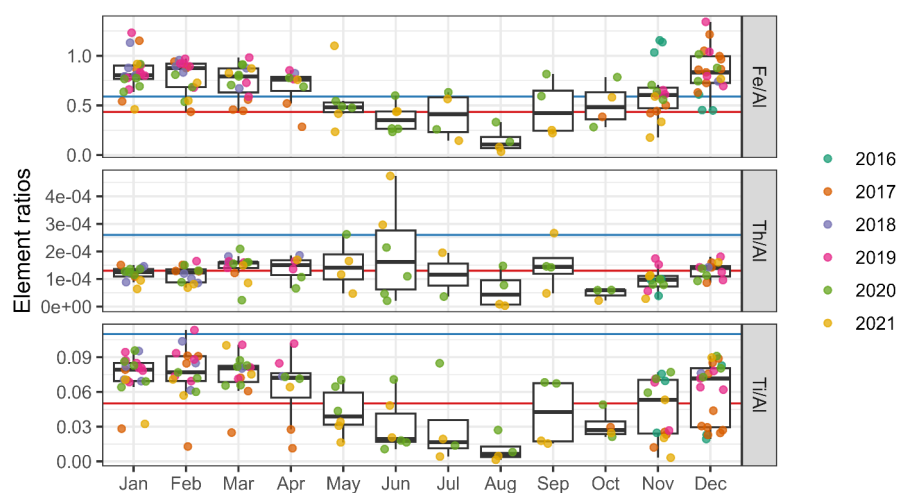
	UCC	Australian soils	kunanyi/Mount Wellington aerosols	
			/UCC	/Australian soil
Al	80400	38560		
Fe	35000	22616	EF(Fe)	1.6 ± 0.6
Th	10.7	10.3	EF(Th)	1.3 ± 2.5
Ti	4100	4313	EF(Ti)	1.2 ± 0.6

285

286 Overall, EFs close to 1 were measured for all aerosol samples, suggesting that the lithogenic tracers
 287 used in this study are indeed of a prevailing crustal origin. Using Australian soil concentration
 288 (Table 1 and supplementary Table S2) to calculate EFs resulted in values further away from the
 289 threshold of 10. In particular, EFs calculated using Australian soil data are closer to 1 for Fe and

a supprimé: ng mg⁻¹

291 Th when compared to using average UCC values (McLennan, 2001). Indeed, underestimated Th
 292 measurements due to incomplete sample digestion (section 2.2) in our study result in a similar
 293 underestimate of EF. Elemental ratio of Ti/Al in aerosol samples collected at kunanyi/Mt
 294 Wellington (Figure 2) were closer to the average ratio of the UCC, resulting in EF(Ti) closer to 1
 295 when compared to using average Australian soil measurement as a reference.
 296



297
 298 **Figure 2.** Boxplot of elemental ratios of Fe/Al (top), Th/Al (middle), and Ti/Al (bottom) in kunanyi/ Mt
 299 Wellington aerosol samples collected between 2016 – 2021, grouped according to month. Whiskers
 300 represent 1.5 times the interquartile range (75th – 25th percentile) beyond the boxes, while the upper, middle,
 301 and lower horizontal lines of the box represent the higher interquartile, median value and lower interquartile
 302 of the average monthly dataset, respectively. Colours represent each sample collection year. Horizontal red
 303 lines represent metal ratios in the average UCC (McLennan, 2001). Horizontal blue lines represent average
 304 metal ratios in the eleven selected NGSAs Australian soil samples (this study). Two Th outliers (May and
 305 June 2020) were excluded from the Th dataset and subsequent calculation for clarity.
 306

307 Mean Al and Fe concentrations measured in our Australian soil samples were both twice smaller
 308 than the average UCC values reported by McLennan (2001) while Ti and Th concentrations were
 309 similar within 10% (Figure 2 and supplementary Table S2). While Australian soil is known for its
 310 high Fe content (Mahowald et al., 2019, Strzelec et al., 2020a), a high soil heterogeneity across
 311 this vast country may explain such surprising observation. This resulted in calculated Th/Al and

312 Ti/Al ratios higher for Australian soil samples while Fe/Al ratios remained similar compared to
313 the average UCC.

a supprimé: significantly

314

315 Elemental ratios calculated for individual aerosol samples are summarised in the supplementary

316 Table S4. Both Fe/Al and Ti/Al ratios showed a clear seasonal trend, with higher ratios resembling

a supprimé: 3

317 mean ratios measured in Australian soil samples (Fe/Al=0.59 and Ti/Al=0.11, Figure 2) in the

318 summertime (December-February) and lower Fe/Al and Ti/Al ratios closer to the average UCC

319 ratios (Fe/Al=0.435 and Ti/Al=0.05, McLennan, 2001) in wintertime (June-August, Figure 2).

320 Summertime Fe/Al ratios in kunanyi/Mt Wellington aerosols were slightly higher (Fe/Al =0.72)

321 than the Australian soil measurements. This can be explained by increased contribution of local

322 soil emission from Tasmania under drier weather conditions as the NGSA database shows higher

a supprimé: and from postfire barren ground. Indeed,

323 Fe/Al ratio (on average 0.7, n=21 samples) in Tasmanian soil compared to other soil across

324 Australia (Caritat and Cooper, 2011; Caritat, 2022). While enhanced air-masses originating from

325 the Australian mainland cannot be observed in the summertime using HYSPLIT model

326 (supplementary Figure S1), the Australian Bureau of Meteorology reports increasing southwards

327 blowing winds at our sampling station from January through to March (supplementary Figure S2).

328 Such discrepancies emphasise the complex regional wind pattern influencing our sampling station

329 and highlight the need to consider other parameters such as seasonal changes in environmental

330 conditions at the source region when investigating aerosol entrainment and transport. Ti/Al ratios

331 were found to lie between our Australian soil (Ti/Al = 0.11) and UCC (Ti/Al = 0.05) references

332 from December through to May, then falling below the UCC ratio in the cooler months of the year.

333 This monthly variability indicates different lithogenic sources of Fe and Ti are likely to influence

334 the atmospheric loading at our sampling station throughout the year. The onset of the dust season

335 on the Australian mainland (October-November, Baddock et al., 2015) may explain part of the

336 summer (dusty) season atmospheric inputs at our kunanyi /Mt Wellington aerosol sampling station,

337 as evidenced by higher Fe/Al (and Ti/Al) ratios in aerosols. On the other hand, other atmospheric

338 sources (locally derived from Tasmania or from long-range transport over the Southern Ocean)

339 with a similar (lower) metal/Al signature than the UCC seem to prevail in our study region during

340 winter. However, the small number of aerosol samples available between May - October in our

341 study does not allow for accurate assessment of trends during the winter period. Much smaller

342 variability was observed for the Th/Al ratio calculated in kunanyi/Mt Wellington aerosols (mean

346 Th/Al = 0.00017) across the time-series, with an overall median ratio close to that of the UCC
347 (mean Th/Al = 0.00013) across most of the year except during August and October.

348

349 Differences between elemental ratios in soil and in aerosol samples may stem from atmospheric
350 processes occurring during transport between source regions and the sampling site including the
351 preferential settling of denser (e.g., oxyhydroxides) minerals over lighter minerals (e.g., clay), and
352 from the mixing of different lithogenic air-masses during atmospheric transport. Analysis of a
353 large set of soil samples, including more locations across Australia and particularly in Tasmania,
354 as well as high resolution information on wind speed and direction at the sampling site and for the
355 duration of the timeseries is necessary to better assess the relative contribution of different
356 Australian dust sources to the lithogenic particulate loading at kunanyi/Mount Wellington.

357

358 3.2 Single tracer lithogenic particle fluxes at kunanyi/Mount Wellington: characteristics 359 and trends

360 Thorium and Ti are commonly used as tracers of lithogenic atmospheric deposition fluxes as they
361 are almost exclusively derived from lithogenic material and have little reactivity or biological
362 utility in the atmosphere (Boës et al., 2001; Ohnemus and Lam, 2015). While Al may be emitted
363 to the atmosphere by anthropogenic sources, its prevailing source in the offshore atmosphere
364 remains crustal material (Xu and Weber, 2021). Although Fe solubility vary following physico-
365 chemical processes during the atmospheric transport, the soluble Fe fraction remains small
366 compared to the total (mostly refractory) fraction of Fe delivered by dust. Hence, if all four tracers
367 have a unique lithogenic source, the use of a multiple tracer lithogenic flux estimate can reduce
368 the uncertainty associated with the variability of a single metal's concentration due to
369 contamination, deviation from the UCC or secondary atmospheric inputs (Traill et al., 2022).

370

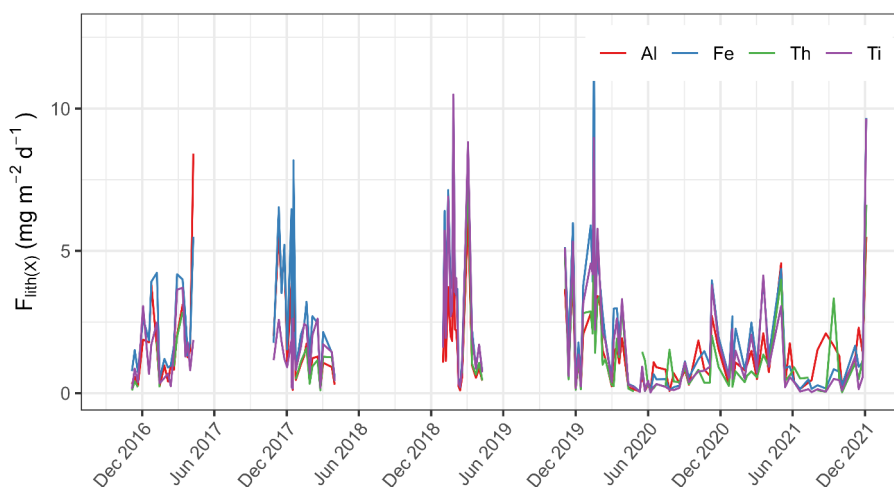
Table 2. Correlation coefficient (R^2) between tracer concentrations in kunanyi/Mount Wellington aerosols.

	Al	Th	Fe	Ti
Al	1	-	-	-
Th	0.90	1	-	-
Fe	0.87	0.82	1	-
Ti	0.74	0.84	0.83	1

371

372 A strong correlation (mostly $R^2 > 0.8$) was found between the total atmospheric concentrations of
 373 Al, Fe, Th and Ti in the individual samples (Table 2). The strongest correlation ($R^2 = 0.90$) was
 374 found between Al and Th and the weakest correlation ($R^2 = 0.74$) was found between total Ti and
 375 Al concentrations in aerosols. Such strong correlations suggest that a common prevailing source
 376 may supply all four tracers to kunanyi/Mt Wellington sampling station. Australian soil samples
 377 collected in the state of Victoria and analyzed in this study also showed a good correlation between
 378 the four lithogenic tracers, with R^2 of 0.97, 0.74 and 0.73 for Fe, Th and Ti when compared to Al
 379 (based on Table S4 data). Such correlation was not found for soil samples from South Australia
 380 (only 2 soil samples from Western Australia). However, the small number of soil sample analysed
 381 in this study ($n=4$ for Victoria and $n=5$ in South Australia) is not sufficient to draw conclusion on
 382 the potential origin of metals in kunanyi/Mt Wellington aerosol samples. The NGS database
 383 available from Caritat and Cooper (2011) also shows a strong correlation (>0.70) between Fe and
 384 Al measurements in soil samples from New South Wales, South Australia and Tasmania using an
 385 aqua regia mineralization and x-ray florescence analysis protocol.

386



387
 388 **Figure 3.** Individual tracer flux, $F_{Lith(X)}$ ($\text{mg m}^{-2} \text{d}^{-1}$), at the kunanyi/Mount Wellington aerosol sampling
 389 station from 2016 to 2021. Data points represent each aerosol mid-sampling period. Gaps in the time series
 390 are periods where samples were not collected due to logistical limitations (winters) or instrument
 391 maintenance. Here, $F_{Lith(X)}$ are calculated using the average UCC content for each metal as reported in
 392 McLennan (2001).
 393

- a supprimé: 3
- a supprimé: No
- a supprimé: significant
- a supprimé: Western Australia and
- a supprimé: .
- a supprimé: for
- a supprimé: the state of
- a supprimé: Indeed, t
- a supprimé: larger
- a supprimé: only
- a supprimé: meaningful correlation
- a supprimé: collected in

a supprimé: Shading denotes every other year starting on 1st of November each year.

408 Dust deposition fluxes estimated using individual tracer (Al, Fe, Th, and Ti) concentrations
409 measured in kunanyi/Mount Wellington aerosols, called $F_{\text{lith}(X)}$, showed similar variability
410 throughout the time-series (2016-2021, Figure 3). Overall, the smallest $F_{\text{lith}(Th)}$ flux was estimated
411 using Th as a single lithogenic tracer, ranging between 0.03 and 7.8 $\text{mg m}^{-2} \text{d}^{-1}$. The largest dust
412 flux was obtained using Fe as a lithogenic tracer and ranged between 0.05 and 12.7 $\text{mg m}^{-2} \text{d}^{-1}$
413 ($F_{\text{lith}(Fe)}$, Figure 3). Lithogenic flux estimates calculated using Al and Ti concentrations in aerosols
414 ranged from 0.06 - 8.4 $\text{mg m}^{-2} \text{d}^{-1}$ and from 0.03 - 10.5 $\text{mg m}^{-2} \text{d}^{-1}$, for $F_{\text{lith}(Al)}$ and $F_{\text{lith}(Ti)}$,
415 respectively. Despite slight differences found between $F_{\text{lith}(X)}$ estimates obtained using different
416 lithogenic tracers, the magnitude of the difference between the highest and lowest $F_{\text{lith}(X)}$ estimates
417 varied by only a factor of 2, which reinforces the likelihood of a common prevailing atmospheric
418 source for all four tracers.

419

420 This finding corroborates work presented by Traill et al. (2022), where concentrations of all four
421 lithogenic tracers showed similar variabilities in marine sinking particles collected in the
422 subantarctic region of the Southern Ocean south of Tasmania (SOTS station). Similarly, Traill et
423 al. (2022) estimated higher lithogenic fluxes when using Fe as a lithogenic tracer and lower
424 lithogenic fluxes when using Th as a lithogenic tracer (Traill et al., 2022). Median $F_{\text{lith}(X)}$ estimates
425 measured at the kunanyi/Mt Wellington sampling site (this study: 1.2, 1.7, 0.8 and 1.1 $\text{mg m}^{-2} \text{d}^{-1}$
426 using Al, Fe, Th and Ti as individual lithogenic tracer, respectively) compares well with reported
427 dust deposition fluxes of 1.4 - 5 $\text{mg m}^{-2} \text{d}^{-1}$ estimated by models in the study region (Jickells et al.,
428 2005; [Mahowald et al., 2005](#); Weis et al., 2024) and other Southern Hemisphere dust fluxes <2.7
429 $\text{mg m}^{-2} \text{d}^{-1}$ reported off the coasts of South Africa and South America, away from major dust
430 sources (Menzel Barraqueta et al., 2019). Our flux estimates are smaller than mineral dust
431 deposition estimates of 4.0 - 25.0 $\text{mg m}^{-2} \text{d}^{-1}$ (based on Ti concentration in aerosols) reported by
432 Strzelec et al. (2020a) in Western Australia, much closer to large Australian deserts.

433

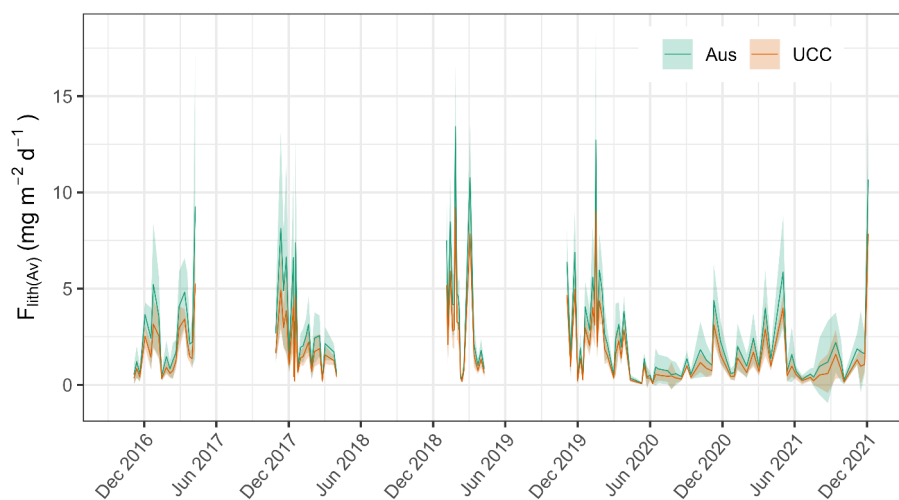
434 Overall, maximum $F_{\text{Lith}(X)}$ estimates in our study were calculated during austral summer months
435 (roughly December – March). Different metals are observed to dominate the summer $F_{\text{Lith}(X)}$ peak
436 each year, with Al showing the highest $F_{\text{Lith}(X)}$ flux in summer 2016/17 (8.4 $\text{mg m}^{-2} \text{d}^{-1}$), Fe in
437 2017/18 (8.2 $\text{mg m}^{-2} \text{d}^{-1}$) and in 2019/20 (12.7 $\text{mg m}^{-2} \text{d}^{-1}$), and Ti in 2018/19 (10.5 $\text{mg m}^{-2} \text{d}^{-1}$)
438 and in 2021/22 (9.6 $\text{mg m}^{-2} \text{d}^{-1}$). This may be due to variabilities in the nature and composition of

439 the dominant dust source arriving at the sampling site each year, including the impact of dust-
440 containing fire emissions during the summer seasons 2018/19 and 2019/20 (Perron et al. 2022).

441

442 3.3 Multi tracer particle flux

443 All four tracers (Al, Fe, Th, and Ti) measured in kunanyi/Mount Wellington aerosols showed a
444 strong correlation with one another and a similar variability over time (section 3.1), suggesting
445 that they originated from a single terrestrial source. This supports the approach taken in this study
446 whereby a multi-tracer lithogenic deposition flux, called F_{LithAv} , is estimated by averaging $F_{Lith(x)}$
447 fluxes obtained using each of the four tracers for each sample. The resulting F_{LithAv} estimated at
448 our station between 2016 and 2021 is displayed in Figure 4 and provides a more robust estimate
449 of deposition flux by smoothing variability between tracers (displayed in Figure 3). Individual and
450 average lithogenic flux estimates ($F_{Lith(x)}$ and F_{LithAv} , respectively) calculated in this study are
451 summarised for individual samples in the supplementary Tables S5 and S6, respectively.



452 **Figure 4.** Multi-tracer lithogenic flux estimate, F_{LithAv} , expressed in $mg\ m^{-2}\ d^{-1}$, corresponding to the average
453 of all individual tracer fluxes ($F_{Lith(x)}$) calculated based on the lithogenic composition of the UCC (orange
454 colour) and that of the eleven Australian soil samples measured in this study (green colour). Shadings
455 represent +/- one F_{LithAv} standard deviation of the average (solid lines).
456
457

458 A mean F_{LithAv} value of $1.8 \pm 1.3\ mg\ m^{-2}\ d^{-1}$ was calculated based on the analysis of aerosol samples
459 collected between 2016 and 2021 at kunanyi/Mt Wellington (Tasmania, Figure 4 orange colour).

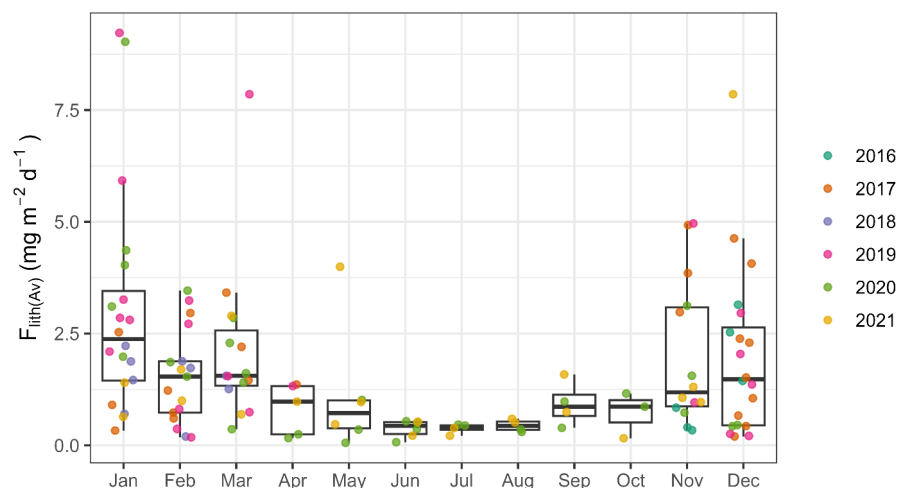
a supprimé: 4
a supprimé: 5
a mis en forme : Interligne : Multiple 1.15 li

462 Throughout our time series, the highest F_{LithAv} values were observed in January 2019 and 2020,
463 with flux peaks reaching 9.2 in January 2019 and 9.0 $mg\ m^{-2}\ d^{-1}$ in January 2020, respectively.
464 Noticeable peak fluxes of 7.9 $mg\ m^{-2}\ d^{-1}$ also occurred in early March 2019 and in mid-December
465 2021. Extended periods of low F_{LithAv} estimates ($\leq 0.5\ mg\ m^{-2}\ d^{-1}$) were observed during the two
466 austral winter periods sampled, with a minimum flux of 0.06 $mg\ m^{-2}\ d^{-1}$ reached in May 2020
467 (Figure 4). There is therefore an apparent seasonal trend in dust deposited at the kunanyi/Mt
468 Wellington site, with higher F_{LithAv} observed in warmer periods (November - March) and lower
469 fluxes in cooler periods of the year (May - August). It should be mentioned that a mean F_{LithAv}
470 value of $2.7 \pm 1.9\ mg\ m^{-2}\ d^{-1}$ is estimated when using the average metal content in Australian soil
471 analyzed in this study (Figure 4 green colour). Indeed, while Th and Ti contained in our eleven
472 Australian soil samples show similar concentrations (within 10%) as in the average UCC
473 (McLennan, 2001), Al and Fe concentrations in these local soil samples differ by 52 and 35%,
474 respectively. This result in higher F_{LithAv} estimated using Australian soil data (Figure 4).

475 The mean F_{LithAv} observed in this study, of 1.8 $mg\ m^{-2}\ d^{-1}$ when using the average UCC and 2.7
476 $mg\ m^{-2}\ d^{-1}$ when using the average Australian soil measurement (Table S5), fall within the dust
477 deposition range of 1.1 - 5.5 $mg\ m^{-2}\ d^{-1}$ reported by models in southeastern Australia, which
478 account for soil erodibility, soil particle size distribution and wind friction velocity (Albani et al.,
479 2014; Weis et al., 2024). In the Southern Ocean south of Tasmania, smaller mineral dust fluxes of
480 0.37 $mg\ m^{-2}\ d^{-1}$ and 1.0 $mg\ m^{-2}\ d^{-1}$ were reported based on aerosol Fe measurements at sea, particle
481 size and surface wind speed (Bowie et al., 2009) and based on Al, Fe, Th and Ti measurements in
482 marine sinking particles (Traill et al., 2022), respectively. Traill et al. (2022) reported a similar
483 annual variability in lithogenic deposition flux at SOTS between 2011 and 2018, with minimum
484 F_{LithAv} around 0.5 $mg\ m^{-2}\ d^{-1}$ in July-September and an earlier dust deposition peak (compared to
485 our study) in November-December, up to 2.5 $mg\ m^{-2}\ d^{-1}$. Strzelec et al. (2020a) also reported (up
486 to 6 times) higher mineral dust fluxes in warmer months compared to cooler months based on Ti
487 analysis in aerosols from Western Australia. In particular, the two summer seasons showing F_{LithAv}
488 over 9.0 $mg\ m^{-2}\ d^{-1}$ correspond to large bushfire seasons in Tasmania and in Australian mainland
489 upwind from Tasmania, respectively (Perron et al., 2022). Indeed, fire events are known to
490 exacerbate dust entrainment into the atmosphere both during (pyro convective updrafts) and post
491 (burnt ground) fire event (Hamilton et al., 2022). It is worth noting that F_{LithAv} estimated using

a supprimé: 3

493 Australian soil measurements (this study) fall closer to the mean reported estimate found in the
 494 literature while using the average UCC value result in lower-end F_{LithAv} estimate compared to the
 495 literature. While F_{LithAv} estimated using the average UCC may present an advantage in being more
 496 comparable with other studies worldwide, F_{LithAv} estimated using Australian soil data may be more
 497 relevant for validating model outputs as it likely better represents true deposition fluxes in our
 498 study region. Overall, the choice of one or the other crustal source result in up to a factor 2
 499 difference in the calculated F_{LithAv} .



500
 501 **Figure 5.** Monthly F_{LithAv} estimates, in $mg\ m^{-2}\ d^{-1}$, based on lithogenic tracer analysis in aerosol samples
 502 collected between 2016-2021 at the kunanyi/Mt Wellington site. Individual (weekly) samples are shown
 503 as dots and the colour code represents each collection year. Whiskers represent 1.5 times the interquartile
 504 range (75th – 25th percentile) beyond the boxes, while the upper, middle, and lower horizontal lines of the
 505 box represent the higher interquartile, median value and lower interquartile of the average monthly
 506 dataset, respectively.

507
 508 Greatest F_{LithAv} fluxes are annually observed during the austral summer (December - March),
 509 with median F_{LithAv} of $2.4\ mg\ m^{-2}\ d^{-1}$ in January and around $1.4\ mg\ m^{-2}\ d^{-1}$ in December,
 510 February and March across all years (Figure 5). This tendency aligns with higher frequency of
 511 dust storms occurring in Australia’s main geological basins during warmer months (late austral
 512 spring and summer), resulting in higher dust deposition fluxes (O’Loingsigh et al., 2017). The
 513 summers of 2017/2018 (Nov-Dec), 2018/19 (Jan-Feb) and 2019/20 (Dec-Feb) had especially
 514 high F_{LithAv} fluxes compared to other summer periods in the time-series (Figure 5). These
 515 observations are consistent with the year 2017 being identified as the third driest year since

a mis en forme : Normal (Web), Gauche, Pas de paragraphes
 solidaires

516 records have been kept in Australia (Steffen et al., 2018), and the two following summer periods
517 being identified as strong bushfire years, across Tasmania in 2018/2019, and across southeast
518 Australia in 2019/2020 (Perron et al., 2022). Relatively smaller peaks were observed during the
519 summer of 2020/21 and, to a lesser extent, during the 2016/17 summer (Figure 5). This may
520 reflect two wetter summer periods under the influence of El Niño Southern Oscillation positive
521 phase (La Niña), where increased moisture in the topsoil restricted particles from being eroded
522 and entrained by air masses (Bureau of Meteorology, 2022). In addition, fewer bushfire
523 emissions during these two wetter summer periods may have resulted in less dust emissions due
524 to increased vegetation cover on the soil (Bureau of Meteorology, 2022). Wetter summer seasons
525 may also explain a shift in F_{lithAv} peaks towards the end of the summer seasons 2016/17 and
526 2020/21 (February - March) compared to the December-January $F_{\text{lith(Av)}}$ peak observed in
527 2017/18, 2018/19, and 2019/20 (Figure 5).
528

529 4. Conclusions

530 This study explores the seasonal and interannual variability of the lithogenic deposition flux using
531 analysis of Al, Fe, Th, and Ti (as lithogenic tracers) in aerosol samples collected at kunanyi/Mt
532 Wellington (Tasmania, Australia). Enrichment factors close to 1 and elemental ratios similar to
533 those measured in soil samples collected in Australian dust source regions confirmed the crustal
534 origin of all four tracers. Deposition fluxes, $F_{\text{Lith}(X)}$, calculated using each tracer individually
535 showed small differences, of a factor 2 on average, between one another throughout the 2016-2021
536 time series. This study suggests the use of a multi-tracer (averaged) dust deposition flux estimate
537 as a more robust method to account for variability of individual tracers in aerosols.

538 The mean F_{lithAv} of $1.8 \text{ mg m}^{-2} \text{ d}^{-1}$ calculated in this study across the 2016-2021 time-series is
539 consistent with earlier lithogenic deposition fluxes reported in the literature. Dust flux maxima (up
540 to $9.2 \text{ mg m}^{-2} \text{ d}^{-1}$) were consistently observed during the austral summer, while minimum annual
541 F_{lithAv} (down to $0.06 \text{ mg m}^{-2} \text{ d}^{-1}$) were estimated in the winter. Overall, individual year F_{lithAv} fluxes
542 aligned well with the occurrence of known dust and bushfire events in the summertime as well as
543 other global meteorological events such as El Niño Southern Oscillation (ENSO) which drive the
544 weather patterns across southeast Australia.

545 Dust deposition fluxes calculated in this study hold some uncertainties -- a factor 3 and a factor 2
546 due to the use of a set deposition velocity and the assumption of metal abundance as per the average
547 UCC, respectively. While using the averaged UCC to calculate F_{lithAv} may present an advantage

548 in being more comparable with other studies worldwide, we show that F_{LithAv} estimates (0.09 –
549 13.4 mg m⁻² d⁻¹) calculated using metal abundance in Australian soils are in better agreement with
550 dust fluxes reported by global models in our study region. Therefore, understanding local soil
551 composition is essential to estimating dust deposition fluxes in different study regions. Overall,
552 the uncertainty in field-based dust deposition flux estimates likely remain smaller than
553 uncertainties associated with model parametrization.

554 As dust deposition is now being recognized as a major source of vital micro-nutrients such as Fe
555 to the Southern Ocean, accurately quantifying dust fluxes is vital to understanding primary
556 production in the Southern Ocean and how this may change under future climate scenarios. Our
557 observed dust flux maxima in austral summer may also provide a much-needed regional pulse of
558 nutrients to phytoplankton when water column nutrients are being depleted through the growing
559 season.

560 Additional observations covering a wider geographical area and greater temporal coverage
561 (including time-series stations and winter sampling periods) are required to better constrain
562 seasonal and interannual variability. Our study adds vital data to the relatively few field-based dust
563 deposition flux estimates available to validate model outputs, especially for Southern [hemisphere](#)
564 dust sources (including [Australia](#)) which greatly vary in nature and composition.

566 Author contributions

567 A.R.B. was responsible for project conceptualisation, funding acquisition, resources and
568 supervision. M.M.G.P. was responsible for part of the sample collection, sample processing, data
569 interpretation, processing and curation as well as for manuscript drafting. S.M was responsible for
570 part of the sample collection and analysis, and for laboratory supervision. T.H was responsible for
571 data curation. C.N was responsible for the analysis of soil samples. C.H was responsible for part
572 of the sample collection, sample processing, data curation and the original draft writing. A.T. was
573 responsible for instrumental analysis. P.dC. was responsible for part of the sample collection and
574 data curation. M.S. was responsible for part of the sample collection and sample processing. All
575 authors were responsible for data interpretation and validation and reviewing and editing the
576 manuscript.

577

578 **Conflicts of interest**

579 There are no conflicts to declare.

580

581 **Acknowledgements**

582 A.R.B would like to thank the Australian Research Council (ARC) for part funding this work under
583 grants FT130100037 and DP190103504. The Australian Antarctic Program Partnership (AAPP)
584 is also acknowledged for support of laboratory costs as part of the Antarctic Science Collaboration
585 Initiative (ASCI000002). Access to ICP-MS instrumentation was made possible through ARC
586 LIEF funding (LE0989539). M.M.G.P was partly supported by ISblue project, Interdisciplinary
587 graduate school for the blue planet (ANR-17-EURE-0015) and co-funded by a grant from the
588 French government under the program "Investissements d'Avenir" embedded in France 2030. Soil
589 samples were provided by The South Australia Drill Core Reference Library and the Geological
590 Survey of South Australia, within the Department for Energy and Mining; many thanks to Anna
591 Petts for assisting with legacy soil data selection and retrieval. The National Geochemical Survey
592 of Australia, which provided the topsoil samples from Western Australia, South Australia, and
593 Victoria, was a collaboration between Federal, States, and Northern Territory geological surveys
594 led by Geoscience Australia (GA) and funded by the Australian Government's Onshore Energy
595 Security Program (2006-2011). We thank GA for making those samples available for the present
596 study. [We are deeply grateful to Dr Marc Mallet \(University of Tasmania\) for providing advice on](#)
597 [air-mass trajectory analysis.](#)

598

599 **Acknowledgment to country**

600 Before the white settlement of lutruwita/Tasmania, kunanyi/Mount Wellington was a prominent
601 feature in the lives of the Moomairremener people for thousands of years and continues to be. We
602 pay our respects to elders' past, present and emerging and are thankful to have been able to study
603 this region.

604

605 **References**

- 606 Albani S, et al. 2014, 'Improved dust representation in the Community Atmosphere Model', *Journal of*
607 *Advances in Modeling Earth Systems*, vol. 6, no. 3, pp. 541–570, doi/10.1002/2013MS000279.
- 608 Anderson RF, et al. 2016, 'How well can we quantify dust deposition to the ocean?', *Philosophical*
609 *Transactions of the Royal Society A: Mathematical, Physical and Engineering Sciences*, vol. 374, no.
610 2081, p. 20150285, doi/10.1098/rsta.2015.0285.
- 611 Baddock M, et al. 2015, 'Drivers of Australian dust: a case study of frontal winds and dust dynamics in
612 the lower lake Eyre basin', *Earth Surface Processes and Landforms*, vol. 40, no. 14, pp. 1982–1988,
613 doi.org/10.1002/esp.3773
- 614 Baker AR, et al. 2016, 'Trace element and isotope deposition across the air–sea interface: progress and
615 research needs', *Philosophical Transactions of the Royal Society A: Mathematical, Physical and*
616 *Engineering Sciences*, vol. 374, no. 2081, p. 20160190, doi/10.1098/rsta.2016.0190.
- 617 Baker AR, et al. 2017, 'Observation- and model-based estimates of particulate dry nitrogen deposition to
618 the oceans', *Atmospheric Chemistry and Physics*, vol. 17, no. 13, pp. 8189–8210, doi.org/10.5194/acp-17-
619 8189-2017.
- 620 Baker AR, Li M and Chance R, 2020, 'Trace Metal Fractional Solubility in Size-Segregated Aerosols
621 From the Tropical Eastern Atlantic Ocean', *Global Biogeochemical Cycles*, vol. 34, no. 6, p.
622 e2019GB006510, doi/10.1029/2019GB006510.
- 623 [Bindu G, et al. 2016, 'Pattern of aerosol mass loading and chemical composition over the atmospheric](#)
624 [environment of an urban coastal station', *Journal of atmospheric and solar-terrestrial physics,*](#)
625 [vol. 138, 10.1016/j.jastp.2016.01.004](#)
- 626 Bowie AR, et al. 2009, 'Biogeochemical iron budgets of the Southern Ocean south of Australia:
627 Decoupling of iron and nutrient cycles in the subantarctic zone by the summertime supply', *Global*
628 *Biogeochemical Cycles*, vol. 23, no. 4, doi/10.1029/2009GB003500.
- 629 Bowler JM, 1976, 'Aridity in Australia: Age, origins and expression in aeolian landforms and sediments',
630 *Earth-Science Reviews*, vol. 12, no. 2–3, pp. 279–310, doi.org/10.1016/0012-8252(76)90008-8.
- 631 Bureau of Meteorology 2022, *ENSO Outlook*, www.bom.gov.au/climate/enso/outlook.
- 632 Caritat P de and Cooper M, 2011, *National Geochemical Survey of Australia: The Geochemical Atlas of*
633 *Australia*, dx.doi.org/10.11636/Record.2011.020.
- 634 de Caritat P de, 2022, 'The National Geochemical Survey of Australia: review and impact',
635 *Geochemistry: Exploration, Environment, Analysis*, vol. 22, geochem2022-032,
636 doi.org/10.1144/geochem2022-032.
- 637 Crawford J, et al. 2021, 'Fingerprinting Australian soils based on their source location', *Atmospheric*
638 *Pollution Research*, vol. 12, no. 3, pp. 173–183, doi.org/10.1016/j.apr.2021.01.007.
- 639 Cudahy T, et al. 2016, 'Satellite-derived mineral mapping and monitoring of weathering, deposition and
640 erosion', *Scientific Reports*, vol. 6, p. 23702, doi.org/10.1038/srep23702.
- 641 Cutter G, et al. 2017, 'Sampling and Sample-handling Protocols for GEOTRACES Cruises', Version 3.0.
- 642 De Deckker P, 2019, 'An evaluation of Australia as a major source of dust', *Earth-Science Reviews*, vol.
643 194, pp. 536–567, doi.org/10.1016/j.earscirev.2019.01.008.
- 644 Duce RA, et al. 1991, 'The atmospheric input of trace species to the world ocean', *Global*
645 *Biogeochemical Cycles*, vol. 5, no. 3, pp. 193–259, doi/10.1029/91GB01778.

646 Hamilton DS, et al. 2022, 'Earth, Wind, Fire, and Pollution: Aerosol Nutrient Sources and Impacts on
647 Ocean Biogeochemistry', *Annual Review of Marine Science*, vol. 14, no. 1, pp. 303–330,
648 doi/10.1146/annurev-marine-031921-013612.

649 Ito A, et al. 2020, 'Evaluation of aerosol iron solubility over Australian coastal regions based on inverse
650 modeling: implications of bushfires on bioaccessible iron concentrations in the Southern Hemisphere',
651 *Progress in Earth and Planetary Science*, vol. 7, no. 1, p. 42, doi.org/10.1186/s40645-020-00357-9.

652 Jickells T, et al. 2005, 'Global Iron Connections Between Desert Dust, Ocean Biogeochemistry, and
653 Climate', *Science*, vol 308, p. 67-71, doi/10.1126/science.1105959.

654 Mackie DS, et al. 2008, 'Biogeochemistry of iron in Australian dust: From eolian uplift to marine
655 uptake', *Geochemistry, Geophysics, Geosystems*, vol. 9, no. 3, doi/10.1029/2007GC001813.

656 [Mahowald NM, et al. 2005, 'Atmospheric global dust cycle and iron inputs to the ocean', *Global*](#)
657 [Biogeochemical Cycles](#), 19(4), GB4025. doi.org/10.1029/2004GB002402.

658 Mahowald NM, et al. 2006, 'Change in atmospheric mineral aerosols in response to climate: Last glacial
659 period, preindustrial, modern, and doubled carbon dioxide climates', *Journal of Geophysical Research:*
660 *Atmospheres*, vol. 111, no. D10, doi/10.1029/2005JD006653.

661 Mahowald NM, et al. 2009, 'Atmospheric Iron Deposition: Global Distribution, Variability, and Human
662 Perturbations', *Annual Review of Marine Science*, vol. 1, no. 1, pp. 245–278,
663 doi/10.1146/annurev.marine.010908.163727.

664 McLennan SM, 2001, 'Relationships between the trace element composition of sedimentary rocks and
665 upper continental crust', *Geochemistry, Geophysics, Geosystems*, vol. 2, no. 4,
666 doi/10.1029/2000GC000109.

667 Menzel Barraqueta J-L, et al. 2019, 'Atmospheric deposition fluxes over the Atlantic Ocean: a
668 GEOTRACES case study', *Biogeosciences*, 16, doi.org/10.5194/bg-16-1525-2019.

669 Ohnemus DC and Lam PJ, 2015, 'Cycling of lithogenic marine particles in the US GEOTRACES North
670 Atlantic transect', *Deep Sea Research Part II: Topical Studies in Oceanography*, vol. 116, pp. 283–302,
671 doi.org/10.1016/j.dsr2.2014.11.019.

672 O'Loingsigh T, et al. 2017, 'Sources and pathways of dust during the Australian "Millennium Drought"
673 decade', *Journal of Geophysical Research: Atmospheres*, vol. 122, no. 2, pp. 1246–1260,
674 doi/10.1002/2016JD025737.

675 Perron MMG, et al. 2020a, 'Assessment of leaching protocols to determine the solubility of trace metals
676 in aerosols', *Talanta*, vol. 208, p. 120377, doi.org/10.1016/j.talanta.2019.120377.

677 Perron MMG, et al. 2020b, 'Origin, transport, and deposition of aerosol iron to Australian coastal waters',
678 *Atmospheric Environment*, vol. 228, p. 117432, doi.org/10.1016/j.atmosenv.2020.117432.

679 Perron MMG, et al. 2021, 'Atmospheric inputs of volcanic iron around Heard and McDonald Islands, Southern
680 ocean', *Environmental Science : Atmospheres*, vol 1, p 508-517, doi.org/10.1039/D1EA00054C.

681 Perron MMG, et al. 2022, 'Trace elements and nutrients in wildfire plumes to the southeast of Australia',
682 *Atmospheric Research*, vol. 270, p. 106084, doi.org/10.1016/j.atmosres.2022.106084.

683 Reimann C, and P Caritat de. 2005. 'Distinguishing between natural and anthropogenic sources for
684 elements in the environment: regional geochemical surveys versus enrichment factors', *Science of the*
685 *Total Environment*, vol 337, p 91-107, doi.org/10.1016/j.scitotenv.2004.06.011

686 Shelley RU, Morton PL and Landing WM 2015, 'Elemental ratios and enrichment factors in aerosols
687 from the US-GEOTRACES North Atlantic transects', *Deep Sea Research Part II: Topical Studies in*
688 *Oceanography*, vol. 116, pp. 262–272, doi.org/10.1016/j.dsr2.2014.12.005.

689 Sprigg RC. 1982, 'Some stratigraphic consequences of fluctuating Quaternary sea levels and related wind
690 regimes in southern and central Australia, In: *Quaternary dust mantles, China, New Zealand and*
691 *Australia*'. Wasson RJ. ed. pp. 211-240. Australian National University: Canberra.

692 Steffen W, Rice M and Alexander D 2017, 'Another record-breaking year for heat and extreme weather',
693 Climate Council of Australia, ISBN 978-1-925573-47-3.

694 Strzelec M, et al. 2020a, 'Atmospheric Trace Metal Deposition from Natural and Anthropogenic Sources
695 in Western Australia', *Atmosphere*, vol. 11, no. 5, p. 474, doi.org/10.3390/atmos11050474.

696 Strzelec M, et al. 2020b, 'Atmospheric Trace Metal Deposition near the Great Barrier Reef, Australia',
697 *Atmosphere*, 11(4), 394, doi.org/10.3390/atmos11040390.

698 Strzelec M, 2020c, 'Source characterisation of atmospheric trace metal deposition around Australia'.
699 University of Tasmania. Thesis. Doi.org/10.25959/100.00035895.

700 Traill CD, et al. 2022, 'Lithogenic Particle Flux to the Subantarctic Southern Ocean: A Multi-Tracer
701 Estimate Using Sediment Trap Samples', *Global Biogeochemical Cycles*, vol. 36, no. 9,
702 doi/10.1029/2022GB007391.

703 [Vecchio M.A., et al. 2024, 'Provenance of mineral dust deposited on Antarctica over the last sixty years](#)
704 [by strontium isotopic analysis of snow from Dome C', *Atm. Env.*, vol 338,](#)
705 [doi:10.1016/j.atmosenv.2024.120850](#)

706 Weis J, et al. 2022, 'Southern Ocean phytoplankton stimulated by wildfire emissions and sustained by
707 iron recycling', *Geophys. Res. Lett.*, vol. 49, p. 1–11, doi:10.1029/2021gl097538

708 Weis J., et al. 2024, 'One-third of Southern Ocean productivity is supported by dust deposition', *Nature*,
709 vol 629, pp. 603–608, doi:10.1038/s41586-024-07366-4

710 Winton VHL, et al. 2015, 'Fractional iron solubility of atmospheric iron inputs to the Southern Ocean',
711 *Marine Chemistry*, vol. 177, pp. 20–32, doi.org/10.1016/j.marchem.2015.06.006.

712 Winton VHL, et al. 2016, 'Dry season aerosol iron solubility in tropical northern Australia', *Atmospheric*
713 *Chemistry and Physics*, vol. 16, no. 19, pp. 12829–12848, doi.org/10.5194/acp-16-12829-2016.

714 Xu H., and Weber T. 2021, 'Ocean dust deposition rates constrained in a data-assimilation model of the
715 marine aluminum cycle', *Global Biogeochemical Cycles*, vol 35 no. 9. doi.org/10.1029/2021GB007049

716